Ceramics International 50 (2024) 23264–23274

Contents lists available at ScienceDirect

Ceramics International

journal homepage: www.elsevier.com/locate/ceramint

Synthesis of (Ti, W, Mo) CN based cermets with different carbides configurations for demanding applications: Study of the crystal structure, microstructure, and mechanical properties

Seyed Mahdi Rafiaei [a,*], Morteza Hadi [a], F. Fernandes [b,c]

[a] Materials Engineering Group, Golpayegan College of Engineering, Isfahan University of Technology, Golpayegan, 87717-67498, Iran
[b] University of Coimbra, CEMMPRE, ARISE, Department of Mechanical Engineering, Rua Luís Reis Santos, 3030-788, Coimbra, Portugal
[c] CIDEM, ISEP - Polytechnic of Porto, Rua Dr. António Bernardino de Almeida, 4249-015, Porto, Portugal

ARTICLE INFO

Handling Editor: Dr P. Vincenzini

Keywords:
Cermet
Nitrogen
Configuration
Hardness
Toughness

ABSTRACT

In this study, based on different element configurations within constant atomic ratio of elements, $(Ti_{0.93}W_{0.07}Mo_{0.07})C$–20%Ni and $(Ti_{0.93}W_{0.07}Mo_{0.07})CN_{0.3}$-20%Ni derived cermets have been synthesized. The basis for the difference in the production route was whether the carbides were formed by carbothermic reaction from the metal oxide together or separately, or in the case of Mo_2C, the carbide is added to the mixture together with the binder after reduction and just before consolidation. Another basis for the difference was whether the cermet was a carbide or a carbonitride. To investigate the influence of the different production routes, the crystal structure, microstructure, and mechanical properties of the cermets produced were examined using XRD, FESEM, STEM, and Vickers indentation. The XRD spectra of all the cermets were found to be very similar to those of TiC-based cermets, indicating that the additive carbides in the TiC or Ti(CN) phases of the cermets dissolve perfectly during the high vacuum sintering process at 1510 °C. The highest toughness (14.65 MPa $m^{1/2}$) was obtained in $(Ti_{0.93}W_{0.07})$ C–8%Mo_2C–20Ni cermets with a core-rim structure. In addition, the use of nitrogen leads to a dramatic reduction in particle size. The use of molybdenum and tungsten in the form of separate carbides had little effect on limiting the expansion of crystal size and grain size compared to the scenario where the dissolution of these elements took place within the primary core-rim structure. However, in terms of hardness and toughness, it was found that, in addition to grain size, the route taken in the addition of molybdenum and tungsten was also important.

1. Introduction

In recent years, the study of composite materials has become very attractive to engineers and scientists due to their wide range of applications [1–4]. Nowadays, different types of composites are favored by researchers, among which cermets have a special place due to their excellent mechanical properties [5–11]. The reinforcement of these composites usually consists of a mixture of compounds of some non-metallic elements such as carbon and nitrogen with metals such as titanium, tungsten, molybdenum, tantalum, and niobium. The literature review shows that TiC-based cermets are promising compounds not only because of their high hardness and thermal shock resistance, but also because of their exceptional chemical stability [12–14]. Moreover, Ti(CN) reinforced cermets are known as one of the most important cermets due to their resistance to erosion and corrosion. Remarkably, this type of resistance results in more durable performance of cermet specimens and the lack of need for their repair. The exceptional properties of Ti(CN) make it a strategic material used in the electronic and automotive industries, composites, refractories, and also cutting tools [15]. In other words, the cermets can be easily tailored to meet the requirements of different industrial applications. Moreover, many parameters such as a strong binder-reinforcement interface, are required to satisfy several criteria for the use of cermets in many advanced applications [16]. Ni/Co metals and their alloys have been used as binder to retain the hard phases, and thus to produce hard materials [17,18]. However, it should be noted that although conventional cermets (such as WC-Co) are hard and tough, they suffer from poor oxidation resistance and insufficient plastic deformation at high temperatures, which limits their use at such

* Corresponding author.
E-mail address: s.rafiaei@iut.ac.ir (S.M. Rafiaei).

https://doi.org/10.1016/j.ceramint.2024.04.050
Received 11 February 2024; Received in revised form 3 April 2024; Accepted 4 April 2024
Available online 6 April 2024

temperatures. Consequently, Ti (CN)–Ni based cermets are preferred to WC-Co cermets for milling and rough machining of steel and hard materials for the following two reasons. Firstly, the surface finish, dimensional accuracy of the parts, and resistance to chipping are better in the former than in the latter. Secondly, the mechanical–physical properties, such as the hardness of Ti (CN) cermets are higher than those of WC cermets. The literature review shows that the use of additive and ternary carbides has significant effects on the microstructure and mechanical properties of the cermets [19–23]. Previous research has shown that the addition of additive carbides can lead to the formation of a typical core-rim structure [24–26]. Compounds such as TaC, NbC, and Mo_2C have been used as additive carbides in industrial grade cermets since it was found that the additive carbides and the core-rim structures surprisingly improved their fracture toughness. Interestingly, Mo_2C is of great importance for the final properties of cermets, as the presence of this compound refines the microstructure and significantly improves their mechanical properties [19]. Furthermore, the synthesis of different cermets with the same amount of elements results in very different microstructures and mechanical properties depending on the affinity of different elements. For example, titanium-tantalum carbonitride, with or without Mo_2C, has been extensively studied. The results in these cermets indicated that varying the atomic ratios and using different production routes, particularly in terms of processing conditions, sintering time, and sintering additives, can result in different microstructures and mechanical properties [27–30]. Also, for a given composition, different production methods can be developed using carbothermic processes, each with different operating efficiencies. In addition, different ways of incorporating additive carbide alongside titanium carbide have also led to variations in the processes. Numerous papers have been published investigating the incorporation of molybdenum carbide and even tungsten carbide as additive carbides [31–33]. At the same time, the in-situ formation of these carbides by reduction of their oxides has been investigated. The question of whether these different approaches result in different microstructural and mechanical properties is therefore a crucial issue. Unfortunately, to the best of our knowledge, there are no comprehensive studies on the production and characterization of the different configurations of these cermets.

Motivated by this contextual backdrop, in this paper, $(Ti_{0.93}W_{0.07})C$–Ni and $(Ti_{0.93}W_{0.07})(C_{0.7}N_{0.3})$-Ni cermets have been synthesized with the reinforcement of Mo_2C additive carbides. Furthermore, based on $(Ti_{0.93}W_{0.07}Mo_{0.07})C$–20%Ni and $(Ti_{0.93}W_{0.07}Mo_{0.07})CN_{0.3}$-20%Ni cermets, different configurations achieved by the constant atomic ratio of elements have been considered. The crystal structure, microstructure, and mechanical properties of the prepared cermets were characterized using XRD, SEM, FIB, STEM, and Vickers hardness tester.

2. Experimental

2.1. Cermets manufacturing

In this article, 8 different cermets were produced according to the composition in Table 1. The production route of the C_x cermets (x = 1–4) is shown in Fig. 1. The process started with the mixing of different powders, their carbothermic reduction, followed by the addition of Mo_2C as an additive carbide and Ni as a binder or only Ni, depending on the starting powders, followed by ball milling processing and finally cold pressing and sintering.

Table 1
List of the produced cermets and corresponding designation.

Cermet designation	Cermet Compound
C_1	$(Ti_{0.93}W_{0.07})C$–8%Mo_2C–20Ni
C_2	$(Ti_{0.86}W_{0.07}Mo_{0.07})C$–20%Ni
C_3	TiC-14.23%WC-8%Mo_2C–20%Ni
C_4	TiC-22.4 %$(W_{0.48}Mo_{0.52})C$–20%Ni
CN_1	$(Ti_{0.93}W_{0.07})C_{0.7}N_{0.3}$-8%$Mo_2C$–20%Ni
CN_2	$(Ti_{0.86}W_{0.07}Mo_{0.07})C_{0.7}N_{0.3}$-20%Ni
CN_3	$Ti(C_{0.7}N_{0.3})$-14.11%WC-8%Mo_2C–20%Ni
CN_4	$Ti(C_{0.7}N_{0.3})$-22.4$(W_{0.48}Mo_{0.52})C_{0.7}N_{0.3}$-20%Ni

The raw materials in samples C_1 to C_4 have been weighed in such a way that the combination of charge materials results in the same atomic ratio of Ti, W, Mo, and C elements in carbide solid solution of the cermets produced by different routes. This similarity in atomic ratio makes the cermets comparable, and the difference in properties can be attributed to the different production route and the way the raw materials are mixed. The atomic ratio values of the four main atoms in cermets C_1 to C_4, apart from Ni which is a binder and is calculated separately, are 86Ti:7W:7Mo/100C (%at) and are considered the same in all four samples, despite the different production routes. For example, in sample C_1, the charge materials have been calculated so that the carbide obtained from the simultaneous carbothermic reduction of TiO_2 and WO_3 together with graphite, with the addition of a certain amount of Mo_2C, has the atomic ratio mentioned above. Or, in the case of sample C_2, these calculations have been carried out for the three oxides TiO_2, WO_3 and MoO_3 and graphite in such a way that if they were all placed together in a carbothermic reduction chamber, the same atomic ratio of 86:7:7/100 between their elements would still be obtained. However, in sample C_3, as shown in Fig. 1, TiO_2 and WO_3 oxides were reduced by carbothermic reaction in separate chambers and mixed with a certain amount of Mo_2C so that the atomic ratio remained the same. Finally, in sample C_4, one chamber was dedicated to the carbothermic reduction of TiO_2 and one to the simultaneous reduction of WO_3 and MoO_3, but the raw material calculations were still such that the same atomic ratio was also produced in the sample C_4. In fact, there is a one-to-one ratio of carbon to titanium in TiC. With the addition of the elements W and Mo, the combined sum of Ti, W and Mo still forms a one-to-one ratio with the carbon atoms. Therefore, there is no need for a subscript for the carbon atom in the designation of the cermet. Conversely, for carbonitrides, where the sum of nitrogen and carbon is expected to be equal to one carbon atom, subscripts are added to the designation of carbonitride cermets to indicate this relationship in the compounds.

The production route of the CNx cermets (x = 1–4) was the same as the Cx cermets, except that the carbothermic reduction step was carried out in a nitrogen atmosphere instead of under vacuum, allowing N to be incorporated into the material. In the case of samples CN_1 to CN_4, the target atomic ratio, which was the same for all samples and on which the raw material weight calculations were based, was 86Ti:7W:7Mo/70C:30 N (%at). The relationship between the amount of nitrogen absorbed and the pressure in the reduction chamber has been established in previous research, some of which has been published. Therefore, as in the description of samples C_1 to C_4, in samples CN_1 to CN_4 the weight of the raw materials for different production routes has been calculated in such a way that the atomic ratio of 5 elements is the same.

As described above, the starting powders were TiO_2, WO_3, MoO_3, Ni, Mo_2C and graphite. These powders were purchased from Sigma Aldrich at the highest purity. Accordingly, the first step in the preparation of all the samples was to mix the starting powders and then grind them using a high energy ball mill at a speed of 250 rpm for a period of 20 h (Pulverisette 7, Fritsch, Germany). The mixtures were mixed with tungsten carbide balls at a weight ratio of 1:40 powder to ball. In addition, a container of tungsten carbide was used for all milling operations. For the simple carbothermic reduction of the C_1 to C_4 samples, the vacuum level reached was 0.133 Pa. In the case of the CN_1 to CN_4 samples, N_2 gas was added to the furnace atmosphere for the synthesis. In this work, the high vacuum used was achieved by means of mechanical and diffusion vacuum pumps. This process was carried out for 1 h at 1500 °C in a precisely controlled furnace. The appropriate additives, including Mo_2C additive carbides and Ni binder, were then added to the reduced powders. The slurry mixture was subjected to steel ball milling in acetone medium for 24 h, followed by oven drying for 48 h. Disc shaped samples of 1 cm diameter were prepared at a pressure of 125 MPa, followed by sintering in a graphite furnace at 1510 °C in ultra-high vacuum at 0.133 Pa for 75

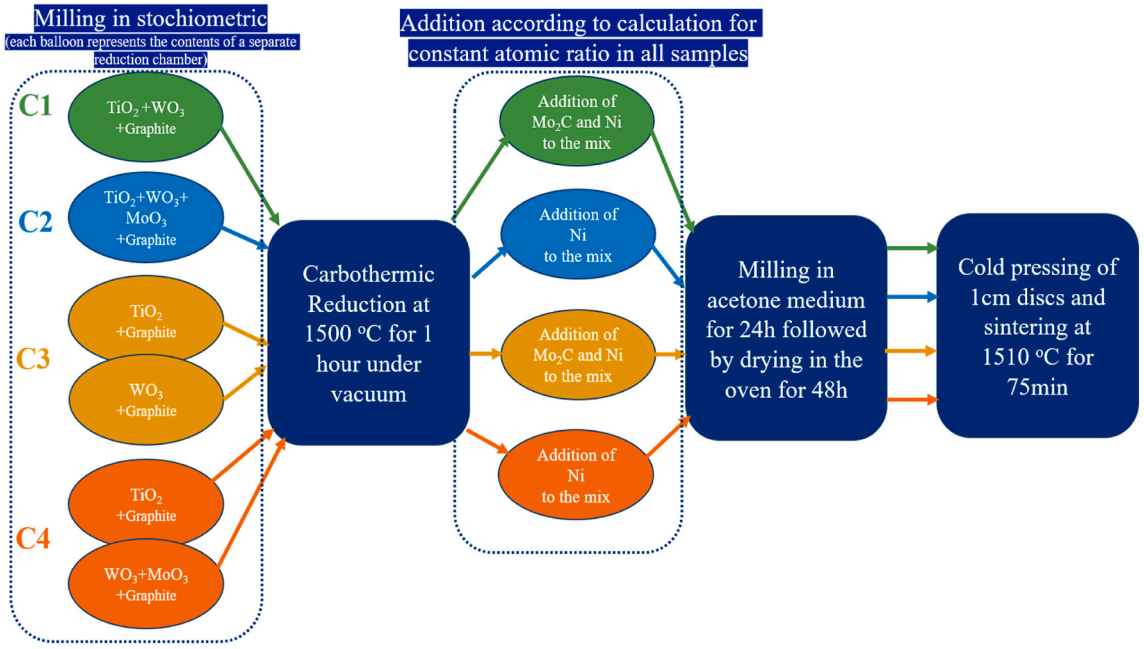

Fig. 1. The different production routes for the samples shown in Table 1, where the production route of cermet C_1 is shown in green, cermet C_2 in blue, cermet C_3 in light brown and cermet C_4 in orange. The production route of cermets CN_1 to CN_4 is like that of cermets C_1 to C_4, with the difference that the carbothermic reduction step is carried out in a nitrogen atmosphere instead of under vacuum. (For interpretation of the references to colour in this figure legend, the reader is referred to the Web version of this article.)

min. The literature review shows that at these high temperatures the binder evaporates and the $(Ti_{1-x}, Mox)_y$ C_z grains suffer oxidation. Therefore, achieving a high vacuum plays an important role in avoiding oxidation [34].

2.2. Characterization

The crystallography of the synthesized cermets was characterized using an X-ray diffractometer (M18XHF-SRA, MacScience, Japan) with monochromatic Cu-Kα radiation (λ = 0.154 nm). The microstructure and chemical composition of the cermets were characterized by scanning electron microscopy (SEM, model JSM-5600, JEOL, Tokyo, Japan). A Hitachi SMI3050SE focused ion beam (FIB) instrument was used to prepare the sample for scanning transmission electron microscopy (STEM) examination. STEM micrographs of the prepared FIB specimens were taken on a JEOL, JEM-2100F instrument while transmission electron microscope (TEM) images were taken on a JEOL JEM-2100 microscope. The hardness of the cermets was measured by the Vickers indentation method using an indenter load of 30 kg (Instron Wilson Hardness, Tukon T 2100B, US) while the fracture toughness was calculated using the expression derived by Shetty et al. [35].

Herein, optical microscope assessments were fulfilled under ambient conditions instantly after indentation to prevent any crack growth. A series of 4 indentations were made for each sample and the average values were reported.

3. Results and discussion

3.1. XRD analysis

Fig. 2 shows the X-ray diffraction (XRD) patterns for the different configurations of carbides and carbonitrides-based cermets. Fig. 2 (a) shows that the produced cermets contain crystallized phases of Ti-based solution carbides which were very close to the titanium carbide (TiC) peaks with a slight shift (ICDD No. 042-1489) and Ni binder (ICDD 96-901-3027) within the produced cermets. Accordingly, the main diffraction peaks observed in the XRD diffraction pattern are the (111), (200), (220), (311), and (222), which belong to the cubic crystal structure of TiC with a lattice parameter of 4.3186 Å, while the strongest peak at 2θ = 42.06 is attributed to the (200) planes. In good agreement with previous research, no tungsten carbide phase was found in the XRD patterns. Investigations have shown that the presence of the tungsten carbide peak on the curve is only observed when they content exceeds a certain threshold (~4 wt%). The formation of carbide or carbonitride solid solutions by sintering has also been reported in previous articles [36]. Furthermore, there are no diffraction peaks associated with oxides, which agrees well with the very low percentages of oxygen element, measured in SEM-EDS analysis. Rong et al. [37] have shown that the use of pure powder and vacuum during carbo-thermic reduction leads to minimal oxygen production in the final cermet and consequently to the production of cermets with crystalline Ni and TiC based phases. It is observed that the different configurations of the carbides resulted in slight peak shifts without the formation of new phases. For the C_1 cermet, the crystalline domain size of 62.3 nm was estimated using the Scherrer equation, $D = 0.9\lambda/\beta\cos\theta$. Where D is the average grain size, and λ is the X-ray wavelength (0.154 nm). In addition, θ and β are the diffraction angle and full width at half maximum (FWHM) of an observed peak, respectively. The XRD spectra of CNx related cermets are like those of TiC-based cermets with a slight shift of the diffraction peaks to higher diffraction angles (compare position of the peaks in Fig. 2a and b). From a structural point of view, the main phases formed in these cermets are similar, which is a remarkable finding and suggests that the dissolution process during cermet manufacturing produces an almost identical solid solution in the structure. Therefore, the phase structural conditions of the cermets were not different from those in the absence of nitrogen.

Despite the different approach to the addition of tungsten and molybdenum carbide and the associated variations, no notable effects on the primary structure have been achieved. The main difference observed in the XRD diffraction peaks, of the carbide and carbonitride compounds, is again the shift of the diffraction peaks to higher angles.

This phenomenon can be well described by the atomic radius of Ti (0.75 Å), W (0.74 Å), and Mo (0.79 Å). Referring to the smaller ionic radius of W than that of Ti, the distance (d) of (200) planes in

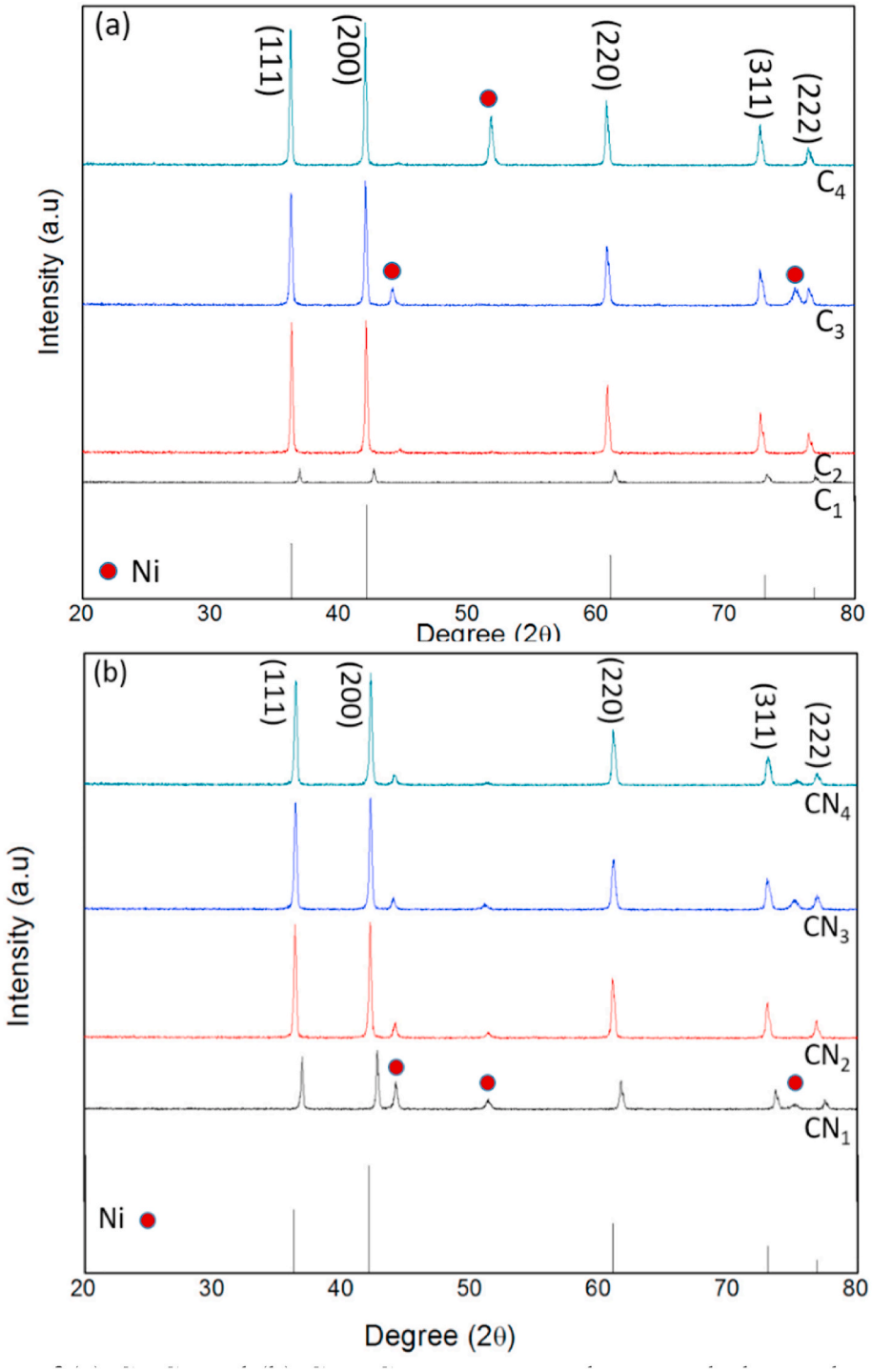

Fig. 2. XRD patterns of (a) C_1–C_4 and (b) CN_1–CN_4 cermets. The crystal planes shown next to the peaks refer to Ti-based solution carbide based on the TiC reference pattern with a slight shift (ICDD No. 042-1489).

($Ti_{0.93}W_{0.07}$) C-based cermets will be smaller than that of TiC based cermets. In addition, since the ionic radius of Mo is larger than that of Ti, the amounts of (200) distances in ($Ti_{0.8665}W_{0.0653}Mo_{0.0682}$) C–20%Ni cermets will be larger than those of ($Ti_{0.93}W_{0.07}$)C–8%Mo_2C–20Ni cermets. Similarly, this issue is consistent for the carbonitrides based cermets (CN_1–CN_4). The outcome demonstrates that the disparity in the configuration of the carbides in an almost equivalent overall composition merely results in dissimilarities in the dissolution rate of elements in the solid solution phase, but not to the formation of new phases.

According to the Scherrer equation, smaller FWHM (see Table 3) indicate coarser particles. The average FWHM for C and CN related cermets are 0.1377 and 0.1525, respectively. The larger FWHM of CN materials is in good agreement with the high thermodynamic stability of CN compounds and the inhibited grain growth of the grains [38]. The distinctions within the FWHM values are not too significant to confirm the effect of controlling growth by varying the conditions of the carbides. For this reason, further investigation using the Rietveld method and microstructural examination is required. However, the average interplanar distance of (200) planes for the C and CN compounds are 2.1437 and 2.1358 Å, respectively (Table 3). The smaller lattice of

Table 2
XRD data of the synthesized cermets.

Cermet	Peak Pos. (2θ)	FWHM (2θ)	Height	d (Å)	Crystallite size (Å)
C_1	42.61	0.19	44.23	2.119	623
C_2	42.03	0.12	723.65	2.15	1467
C_3	41.95	0.12	453.31	2.15	1467
C_4	41.95	0.12	770.11	2.15	1464
CN_1	42.69	0.09	211.65	2.12	2245
CN_2	42.12	0.16	409.77	2.14	878
CN_3	42.16	0.14	409.17	2.14	1092
CN_4	42.15	0.22	379.64	2.14	546

Table 3
Average amounts of FWHM, d-spacing, and crystalline domain sizes of C and CN based cermets.

Cermets	FWHM	d-spacing (Å)	Crystalline domain size (Å)
C	0.14	2.1437	1255.25
CN	0.15	2.1358	1190.25

CN-based cermets is a result of slower crystal growth during the sintering process at 1510 °C. This scenario is consistent with the larger average crystalline domain size of the C-based cermets which was reported by Rafiaei et al. [19] who investigated the effect of nitrogen on the grain size growth and found that the use of nitrogen resulted in higher grain stability.

The Rietveld calculation of different configurations of cermets was carried out using MAUD software (see Fig. 3). Obviously, it is easy to see that the diffraction patterns of the produced cermets agree well with the Crystallographic Information Framework (CIF) of TiC carbide and also Ni binder (CIF No. 1011320 & 2100661). Given that the sig parameters of the Rietveld refinements of C_1, CN_1, C_2, and CN_2 cermets are 0.8, 1.81, 1.16, and 1.87, respectively, one can expect that since they are less than 2, the goodness of fit (GOF) has been acceptable.

The calculated crystalline domain sizes of C_1, CN_1, C_2, and CN_2 cermets are 623, 2245, 1467, and 878 Å, respectively. The crystalline domain sizes of carbide-based cermets are higher than those of the carbonitride cermets. Although the results obtained for crystalline domain size changes as described agree with the lattice strain results calculated by Rietveld, the calculation of crystalline domain size using this method may have a negligible error.

The calculated microstrains of C1, CN_1, C_2, and CN_2 cermets are 0.00058, 0.00083, 0.0005, and 0.00095, respectively. It is noteworthy that the microstrains of CN_1 and CN_2 cermets are significantly higher than those of C_1 and C_2. In fact, the addition of nitrogen leads to the suppression of crystal growth and the remaining microstrain will be higher, which is like the results reported by Yu et al. [39]. In other words, through the explained carbothermic processes, the increase in crystalline domain size leads to the release of microstrain.

Furthermore, the XRD spectra of all the cermets are very similar to those of TiC-based cermets. This means that the dissolution of W and Mo elements in TiC carbide cannot significantly produce any additional peak in the XRD spectra [40]. Since no peaks related to the additive carbides are detected, it is logical to assume that the additive carbides are completely dissolved in the TiC/Ti(CN) solid solution formed in the microstructure of the cermets during the sintering process at 1510°C. Since the strongest diffraction peaks of Mo_2C (ICDD No. 00-001-1188) and WC (ICDD No. 00-002-1055) occur at 2θ of 35.89/39.49 and 48.65 respectively, it can be assumed that the declared diffraction peaks of TiC do not show any overlap with those of other present carbides.

3.2. Microstructure analysis

To understand the carbide coalescence phenomenon, different cermets of the same composition were synthesized. The study of the carbothermic reduction of TiO_2, WO_3 and MoO_3 oxides and their conversion to carbide, which requires the study of thermal behavior with DSC-TG and reduction reactions, has been published in previous articles [41–43]. The microstructure of the C-based cermets is shown in Fig. 4. Firstly, it is easy to see that carbide cermets microstructures without nitrogen mainly have a core/rim type morphology. Notably, the literature review indicates that core/rim structures tend to provide good mechanical properties [44]. While some studies have reported the segregation of metal elements in the rim and observed an inverse contrast [45], and in some cases the removal of the core/rim structure from the cermet microstructure has been documented [46], the results of our research show the formation of the typical core/rim structure. This structure is consistent with observations reported in other articles on this type of cermet. The core-rim structure in carbide cermets is typically formed during the sintering process. It occurs because certain elements within the material diffuse preferentially towards the edges. During sintering, particles in the material start to stick together and as the temperature rises, atoms from different elements move around. This movement isn't uniform; certain atoms tend to move towards the edges of the particles, resulting in a concentration of certain elements at the edges. This concentration forms the rim around each particle, resulting in the characteristic core-rim structure observed in carbide cermets [19]. In addition, the formation of inner and outer rims in the microstructure of the cermets was not detected. Inner and outer rim in carbide cermets refer to regions of different microstructural characteristics near the core, typically characterized by differences in composition [47]. Secondly, although the dimensions of the primary particles after the carbothermic process were in the nanoscale range, the size of the cores in all samples is larger than the nanoscale. This is due to the high temperature sintering used which caused the increase in features. The EDX spectra show that the core (A) and rim (B) regions contain Ti/W/C and Ti/W/Mo/C elements respectively. It is interesting to note that the percentage of Ti element in A is higher than that of in B. Taking this into account we can conclude that the Mo element replaces Ti sites in the rim structure, causing the complete dissolution of Mo in the lattice. It can also be seen that samples C_1 and C_2 have a smaller core size than samples C_3 and C_4. This can be explained by the fact that in the production route of samples C_1 and C_2, TiO_2 and WO_3 were ground in a single grinding chamber prior to carbothermic reduction, whereas in samples C_3 and C_4, these two oxides were ground separately (Fig. 1). Therefore, this difference can be interpreted by considering that a finer particle size can be obtained by grinding a mixture of two oxide brittle materials together under brittle-brittle conditions.

Fig. 4a and b shows that the microstructure of the C_2 cermet is relatively smaller than that of the C_1 cermet. This can be explained by the suppression of the dissolution of Mo in the structure during sintering. In fact, a comparison of Fig. 4a and b indicates that the core size of the $(Ti_{0.93}W_{0.07})$ C-based cermets is extremely larger than that of $(Ti_{0.86}W_{0.07}Mo_{0.07})$ C cermet. $(Ti_{0.86}W_{0.07}Mo_{0.07})$ C based cermets experience less coalescence and are thermodynamically more stable. On the contrary, the energy state of $(Ti_{0.93}W_{0.07})$ C based cermets tends to be reduced by significant particle growth. It seems that the presence of molybdenum soluble element in the composition of ternary carbide inside the core reduces the diffusion ability of atoms and with the reduction in diffusion rate, the growth of the core occurred less in C_2 sample than in C_1 sample. Furthermore, the cermets containing separate TiC, WC, and Mo_2C carbides have a larger core size after the sintering procedure at high temperatures (see Fig. 4c). Finally, it was found that the microstructures of C_3 and C_4 are very similar, which explains that the cermets containing the combination of TiC, WC and Mo_2C carbides have an analogous coalescence behavior to the cermets containing $(W_{0.48}Mo_{0.52})$ C carbides. In other words, it can be interestingly concluded that the formation of $(W_{0.48}Mo_{0.52})$ C complex carbide does not change the energy state and thermodynamic stability of the cermets including TiC, WC and Mo_2C carbides (see Fig. 4c and d).

Since the microstructure of carbonitride based cermets is

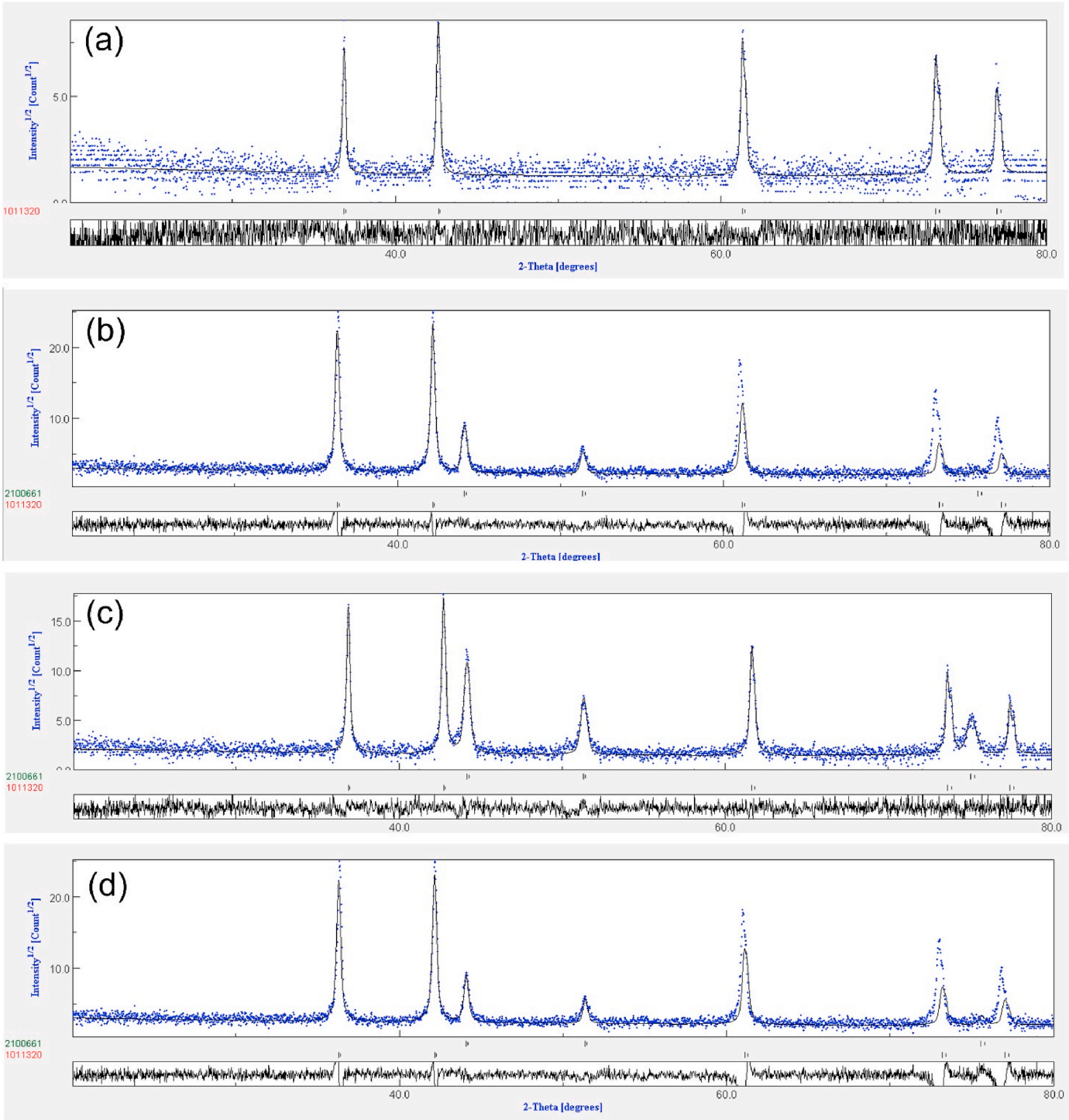

Fig. 3. Rietveld analysis of XRD data of (a) C_1, (b) CN_1, (c) C_2, and (d) CN_2 cermets.

significantly smaller than that of the carbide based cermets, STEM microscopy was used to monitor the size of the carbonitride based cermets. Fig. 5 shows the results of the STEM characterization of the CN_1–CN_4 cermets produced. It can be concluded that the microstructure of the CN_1 cermet is much larger than that of CN_2 (see Fig. 5a and b). This finding is consistent with the FWHM changes in the XRD pattern. In Table 2, the marked variation within the FWHM value in samples CN_1 and CN_2 suggests that the dissolution of molybdenum within the primary solid solution or its presence as a separate carbide positively influences the control of the growth processes. In other words, although carbide solid solution was observed in the final structure of all samples in XRD, and the reason was that in all samples sintering causes dissolution of carbide elements in the core, the differences in the way raw materials are added in samples $CN_1$and CN_2 (see Fig. 1) caused differences in growth. The results show that when molybdenum is formed as a carbide in situ during the carbothermic process together with tungsten and titanium carbide (see C_2 production route in Fig. 1), it is more effective than when it is added to the mixture as a separate carbide (see C_1 production route in Fig. 1). These images show that, in terms of core size, the carbides of CN_2 sample grew less than those of CN_1. Furthermore, from Fig. 5 c-d, it is easy to see that the microstructure sizes of the CN_3 and CN_4 samples are very similar. The comparison of Figs. 4 and 5

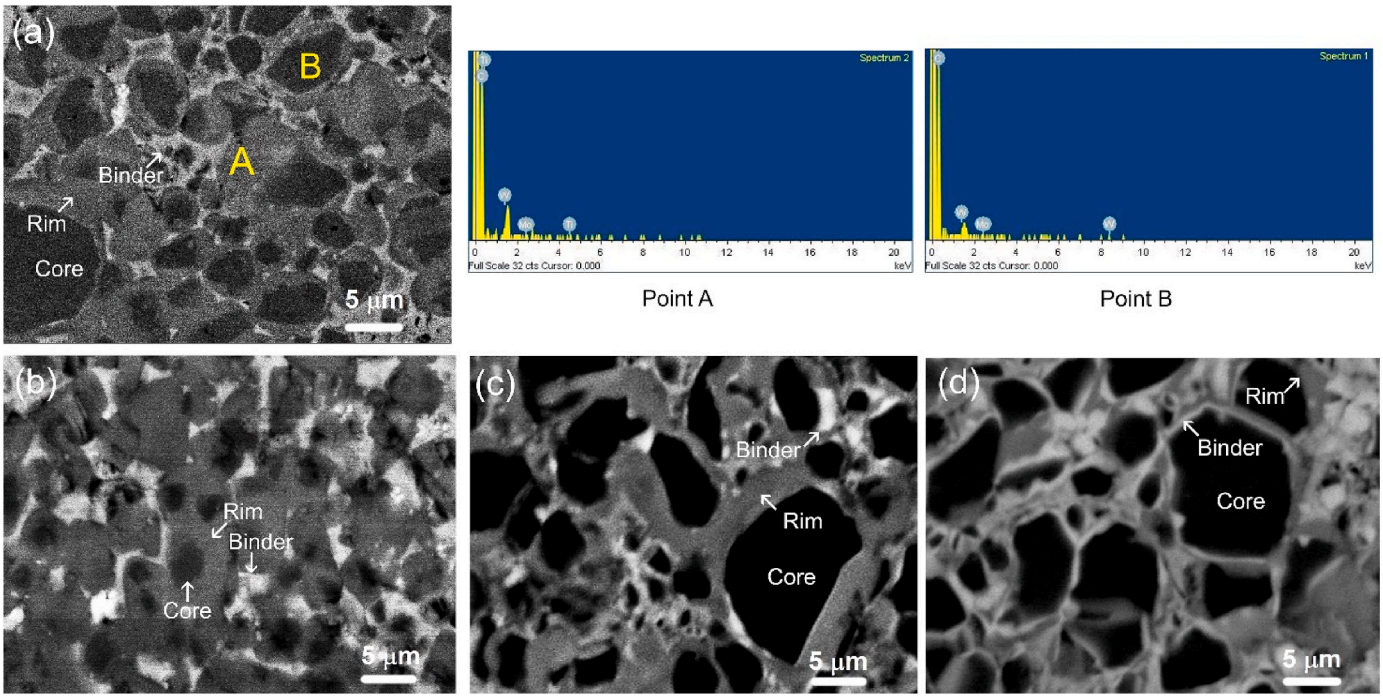

Fig. 4. FESEM images of (a) C_1 with EDS results of two points marked in the figure, (b) C_2, (c) C_3 and (d) C_4. Three parts of the microstructure including core (black regions), rim (grey regions), and binder (white regions) are identified in each image. The designations C_1 to C_4 are given in Fig. 1 and Table 1.

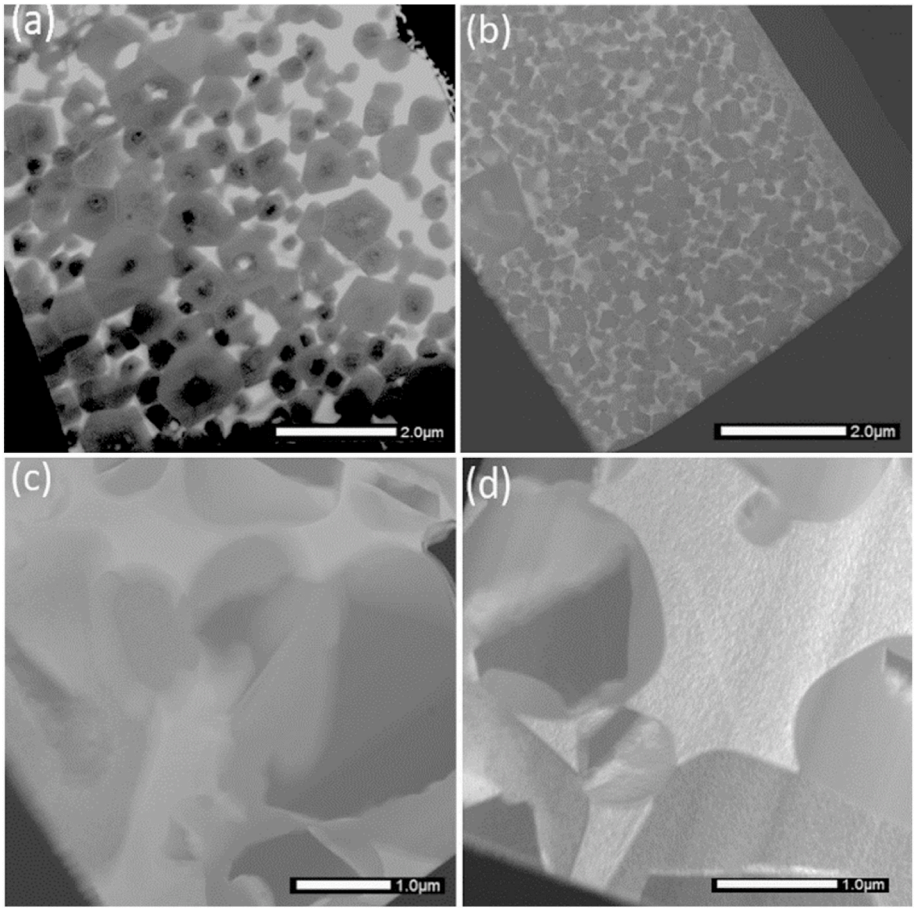

Fig. 5. STEM images of (a) CN_1, (b) CN_2, (c) CN_3 and (d) CN_4 showing that sample CN_2 has the smallest core size among the carbonitride-based cermets. The designations CN_1 to CN_4 are given in Fig. 1 and Table 1.

also suggests that the average core sizes of CN_1–CN_4 are significantly smaller than those of the C_1–C_4 cermets. This issue is attributed to the fact that the presence of nitrogen leads to a decrease in the TiC coalescence tendency. The literature shows that the increase of nitrogen leads to higher stability and then slower growth of $Ti(C_{1-x}N_x)$ than TiC compounds in the melt environment during sintering [19]. Interestingly the sizes of the carbide and carbonitride-based cermets are found to be in reasonable agreement with the calculated crystalline domain sizes of the cermets.

Fig. 6 shows the TEM images of cermet materials CN_1, CN_2, CN_3, and CN_4. Within the STEM investigation, the ability to distinguish the backscattered electrons has demonstrated the disparity in atomic numbers in the core, rim, and binder domains of the microstructural components in the cermets, but the grain size is still not clear. However, with higher resolution TEM, the total grain size can be clearly determined. Again, we see that samples CN_1 and CN_2 have smaller particle sizes compared to CN_3 and CN_4. In addition, the grain size in CN_2 is smaller than that observed in CN1. Both findings are consistent with the microstructures obtained by STEM examination. From the first comparison it can be concluded that the separation of the carbothermic reduction of the tungsten oxide from that of the titanium oxide, (see the production routes of samples CN_3 and CN_4), impairs the result of the fine graining. The second comparison between CN_1 and CN_2 suggests that Mo is more effective in controlling particle size when it is incorporated into the structure by carbothermic reduction rather than when added as an additional carbide. This idea was confirmed by examining the crystal size, core size and grain size. Given the similarity of the phases in the XRD pattern, the main dissimilarity between the two situations above is the distribution of atoms within the final core-rim structure in cermet, which can produce phases with different hardness values. The influence of this diversity in phase arrangement on the overall hardness and toughness of the cermet is considered in the following section. Furthermore, it can also be seen that there is no discontinuity between the grains and the binder. Since the nickel metal has completely enveloped the ceramic particles, it can be expected that the sintering of cermet materials has been successful at very low pressure. The discontinuity has been found to have the potential to cause material failure under thermal or mechanical stress due to stress accumulation at these interfaces [48,49].

3.3. Mechanical properties

Fig. 7 shows the mechanical properties of the cermets produced. It is noteworthy that the hardnesses of all the synthesized cermets are very high, in the range of 11.9–14.4 GPa, which makes them suitable for many advanced applications. To evaluate the variation of the mechanical properties, the introduced values of hardness and toughness were also compared using column plots. It is easy to see that the average hardness of the carbide-based cermets is 12.41 GPa, while that of the carbonitride-based cermets is 13.79 GPa. The introduction of nitrogen into the carbide cermets results in a significant increase in hardness. This result agrees with the microstructures obtained, while it has been observed that C_1–C_4 cermets have relatively larger grain sizes than CN_1–CN_4.

Furthermore, the average toughness of the C_1–C_4 and CN_1–CN_4 cermets is 13.77 and 12.55 (MPa. $m^{1/2}$), respectively, which is in good agreement with our microstructural observations. As explained elsewhere, the high toughness is due to the excellent bonding between the

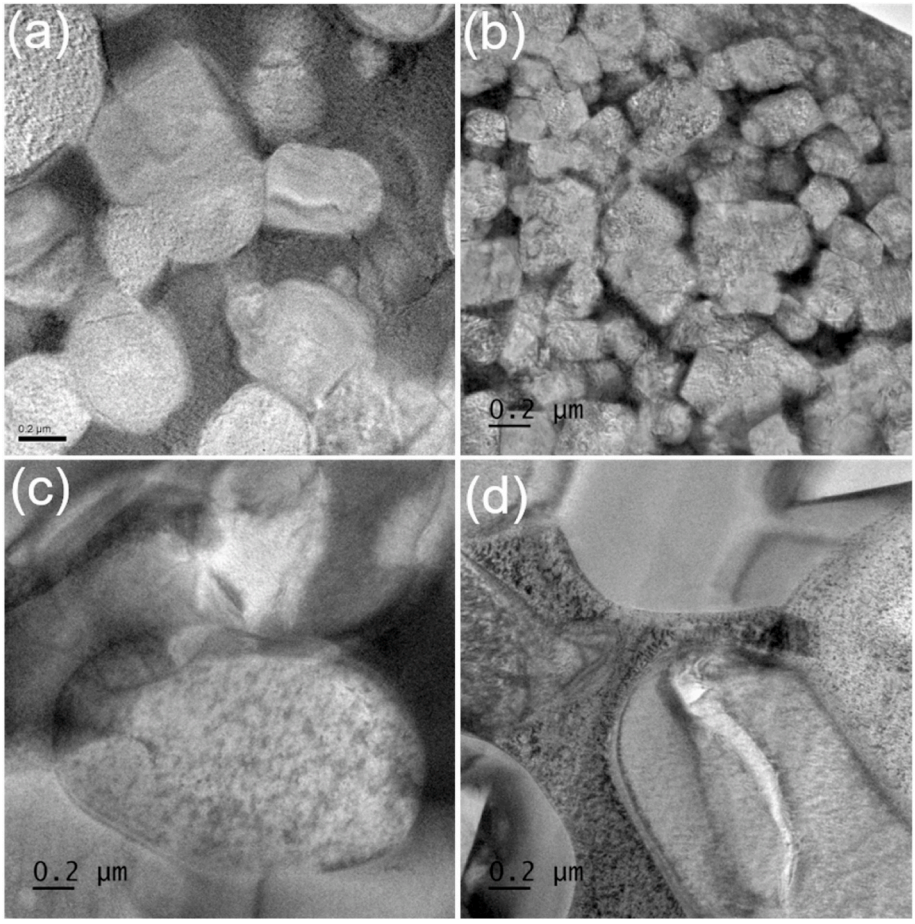

Fig. 6. TEM images of (a) CN_1, (b) CN_2, (c) CN_3 and (d) CN_4 cermets showing that the CN2 sample has the smallest grain size among the carbonitride-based cermets. The designations CN_1 to CN_4 are given in Fig. 1 and Table 1.

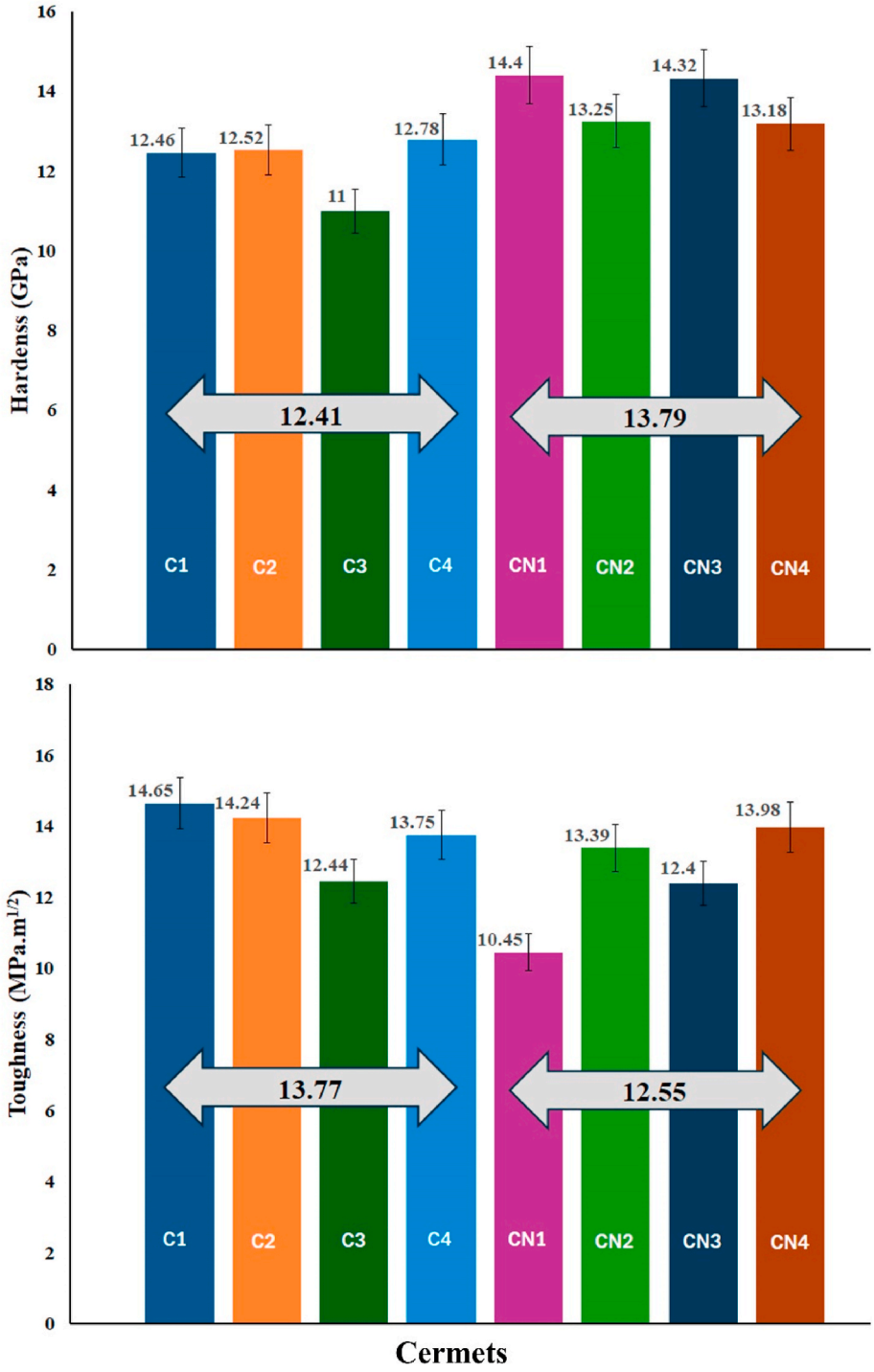

Fig. 7. Hardness and toughness of C1–C4 and CN1–CN4 cermets.

ceramic particles and the metallic binders. Thus, the use of carbides reinforced cermets is an effective way of producing more flexible components with relatively lower hardness values is efficiently achieved. When the hardness data in Table are compared with the results obtained from the microscopic evaluation, although they are largely in agreement, there are some inconsistencies. In other words, the mechanism of increasing hardness with decreasing grain size does not fully explain the results obtained in the hardness evaluation. This is because microscopic analysis revealed that the grain size of CN_1 and CN_2 is smaller than that of CN_3 and CN_4. The reason for this is that the increase in hardness just due to grain size reduction alone is not sufficient to demonstrate the mechanical behavior of the variety of cermets produced during this research. It has been previously reported in other research on ceramic composites that the effect of different factors together on the hardness value can break the expected trend. This is because, in addition to grain size, other factors such as sintering temperature and pressure (which were the same for all samples in this research), milling time, powder morphology and final cermet microstructure affect the hardness values [50]. It seems that the change in the production route has caused the change in the latter two characteristics in the different samples of this research and has affected the hardness.

It has also been found that the orientation of the grains in composites

can be affected by changes in the production parameters, and this different growth orientation of the grains can result in different hardness and strength in the composite [51,52]. Meanwhile, it has been found in previous research that the way of adding secondary carbide has a direct role on the growth of the main carbide grains, so it seems that the variation of hardness obtained is reasonable considering the variation of the way of adding secondary carbides in this work. In addition, it has been reported in the field of other composites that special distribution characteristic of the second phase can be beneficial to the significant improvement of mechanical properties [51,53]. From this point of view, the different production routes for the addition of WC and Mo2C to the TiC matrix in this work could also have affected the hardness, providing a variety of hardnesses for the cermets in the different routes.

Another factor that appears to have a clear effect on the final hardness of carbonitride-based cermets is the way in which the molybdenum and tungsten elements are added in the production route. This different scenario for the addition of Mo and W to the cermet composition results in a different distribution of elements in the core-rim microstructure and, as a result, the overall hardness of CN_1 and CN_3 cermets is greater than that of CN_2 and CN_4 cermets. It has been shown that the hardness of cermets is directly influenced by the type and volume fraction of phases contained in the microstructure [54–56]. In other words, the addition of molybdenum in the form of addition carbide and tungsten by a separate reduction route, rather than addition by simultaneous reduction, although destructive in controlling grain growth, increases hardness, although this simultaneous modification has reduced fracture toughness within these samples. Another possibility is that in specimens with a bulkier core, the hardness indentation lands exclusively in the core rather than in the core and binder material, and therefore, a higher average hardness is recorded in these specimens.

As the cermets usually suffer from low flexibility, the toughness obtained must be considered as an important criterion. The highest toughness of the carbide-based cermets belongs to C_1 with a core-rim structure, which promises outstanding properties of $(Ti_{0.93}W_{0.07})$ C–8%Mo_2C–20Ni cermets. However, this is from the point of view of mechanical properties, and the result may be different from examining other properties of the cermet [57]. Similarly, among the carbo-nitride cermets, CN_4 has the highest toughness, which is well related to its large core-rim morphology. Since each of the eight samples has the minimum hardness required for a durable material in common applications, from a toughness point of view, these two samples can be regarded as the optimum variants in this mixture for (Ti,W)C-based cermets.

4. Conclusion

This study showed that the use of nitrogen leads to a dramatic reduction in particle size. The results revealed that the use of molybdenum and tungsten in the form of separate carbides had little effect on limiting the expansion of crystal size and grain size compared to the scenario where the dissolution of these elements took place within the primary core-rim structure. However, in terms of hardness and toughness are concerned, it was found that, in addition to particle size, the condition regarding the addition of molybdenum and tungsten was also important. In the case of carbonitride cermets, the hardness is approximately 1 GPa higher and the toughness is reduced by up to 3 MPa $m^{1/2}$ when these elements are added as a separate phase carbide. It was found that the average hardness of carbide-based cermets is 12.41 GPa, whereas this value reaches 13.79 GPa, after nitrogen doping. In short, it was concluded that among carbide and carbonitride cermets, C_1 and CN_4 respectively have optimum mechanical properties.

CRediT authorship contribution statement

Seyed Mahdi Rafiaei: Writing – original draft, Supervision, Software, Methodology, Investigation, Formal analysis, Data curation, Conceptualization. **Morteza Hadi:** Writing – review & editing, Validation, Methodology, Investigation, Data curation. **F. Fernandes:** Writing – review & editing, Validation, Investigation, Funding acquisition, Data curation.

Declaration of competing interest

The authors declare that they have no known competing financial interests or personal relationships that could have appeared to influence the work reported in this paper.

Acknowledgement

Filipe Fernandes acknowledges the: UIDB/00285/2020 and LA/P/0112/2020 projects, sponsored by FEDER Funds through Portugal 2020 (PT2020), by the Competitiveness and Internationalization Operational Program (COMPETE 2020), and national funds through the Portuguese Foundation for Science and Technology (FCT).

References

[1] Y. Wu, J. Chen, L. Zhang, J. Ji, Q. Wang, S. Zhang, Effect of boron on the structural stability, mechanical properties, and electronic structures of γ′-Ni3Al in TLP joints of nickel-based single-crystal alloys, Mater. Today Commun. 31 (2022) 103375.
[2] Z. Huang, Y. Zhang, H. Wang, J. Li, Improved electrical resistivity-temperature characteristics of oriented hBN composites for inhibiting temperature-dependence DC surface breakdown, Appl. Phys. Lett. 123 (2023).
[3] H. Ahmadian, T. Zhou, M. Abd Elaziz, M.A. Al-Betar, A. Sadoun, I. Najjar, A. Abdallah, A. Fathy, Q. Yu, Predicting crystallite size of Mg-Ti-SiC nanocomposites using an adaptive neuro-fuzzy inference system model modified by termite life cycle optimizer, Alex. Eng. J. 84 (2023) 285–300.
[4] Y. Li, X. Jiang, X. Wang, Y. Leng, Integration of hardness and toughness in (CuNiTiNbCr) Nx high entropy films through nitrogen-induced nanocomposite structure, Scripta Mater. 238 (2024) 115763.
[5] X.-Q. Zheng, Y. Liu, Slurry erosion–corrosion wear behavior in SiC-containing NaOH solutions of Mo2NiB2 cermets prepared by reactive sintering, Int. J. Refract. Metals Hard Mater. 78 (2019) 193–200.
[6] E. Ghasali, T. Ebadzadeh, M. Alizadeh, M. Razavi, Mechanical and microstructural properties of WC-based cermets: a comparative study on the effect of Ni and Mo binder phases, Ceram. Int. 44 (2018) 2283–2291.
[7] E. Tejado, M. Dias, J.B. Correia, T. Palacios, P.A. Carvalho, E. Alves, J.Y. Pastor, New WC-Cu thermal barriers for fusion applications: high temperature mechanical behaviour, J. Nucl. Mater. 498 (2018) 355–361.
[8] J. Zhang, Y. Zheng, J. Chen, W. Zhou, Y. Zhao, P. Feng, Microstructures and mechanical properties of Mo2FeB2-based cermets prepared by two-step sintering technique, Int. J. Refract. Metals Hard Mater. 72 (2018) 56–62.
[9] S. Hong, Y. Wu, W. Gao, J. Zhang, Y. Zheng, Y. Zheng, Slurry erosion-corrosion resistance and microbial corrosion electrochemical characteristics of HVOF sprayed WC-10Co-4Cr coating for offshore hydraulic machinery, Int. J. Refract. Metals Hard Mater. 74 (2018) 7–13.
[10] H. Kumar, C. Chittosiya, V. Shukla, HVOF sprayed WC based cermet coating for mitigation of cavitation, erosion & abrasion in hydro turbine blade, Mater. Today: Proc. 5 (2018) 6413–6420.
[11] R. Fernandez, B. Jodoin, Cold spray aluminum–alumina cermet coatings: effect of alumina content, J. Therm. Spray Technol. 27 (2018) 603–623.
[12] J. Kim, S. Kang, Microstructure evolution and mechanical properties of (Ti0. 93W0. 07) C–xWC–20Ni cermets, Mater. Sci. Eng., A 528 (2011) 3090–3095.
[13] S. Lemboub, S. Boudebane, F. Gotor, S. Haouli, S. Mezrag, S. Bouhedja, G. Hesser, H. Chadli, T. Chouchane, Core-rim structure formation in TiC-Ni based cermets fabricated by a combined thermal explosion/hot-pressing process, Int. J. Refract. Metals Hard Mater. 70 (2018) 84–92.
[14] A. Rajabi, M. Ghazali, A. Daud, Chemical composition, microstructure and sintering temperature modifications on mechanical properties of TiC-based cermet–A review, Mater. Des. 67 (2015) 95–106.
[15] M. Dios, I. Kraleva, Z. González, P. Alvaredo, B. Ferrari, E. Gordo, R. Bermejo, Mechanical characterization of Ti (C, N)-based cermets fabricated through different colloidal processing routes, J. Alloys Compd. 732 (2018) 806–817.
[16] Z. Fathipour, M. Hadi, M.R. Maleki, F. Fernandes, Effect of binder on oxidation properties of tungsten carbides: a review by a conceptual classification approach, Ceramics 7 (2024) 166–191.
[17] H. Hosseini-Tayeb, S.M. Rafiaei, Effects of lateral and vertical ultrasonic vibrations on the microstructure and microhardness of Stellite-6 coating deposited on Inconel 718 superalloy through laser metal deposition, Mater. Res. Express 7 (2020) 016531.
[18] H. Hosseini-Tayeb, S.M. Rafiaei, Enhanced microstructural and mechanical properties of Stellite/WC nanocomposite on Inconel 718 deposited through vibration-assisted laser cladding, Int. J. Miner. Metall. Mater. 29 (2022) 327–334.
[19] S.M. Rafiaei, J.-H. Kim, S. Kang, Effect of nitrogen and secondary carbide on the microstructure and properties of (Ti0. 93W0. 07) C–Ni cermets, Int. J. Refract. Metals Hard Mater. 44 (2014) 123–128.

[20] C. Park, S. Nam, S. Kang, Enhanced toughness of titanium carbonitride-based cermets by addition of (Ti, W) C carbides, Mater. Sci. Eng., A 649 (2016) 400–406.
[21] H. Yu, Y. Liu, Y. Jin, J. Ye, Effect of secondary carbides addition on the microstructure and mechanical properties of (Ti, W, Mo, V)(C, N)-based cermets, Int. J. Refract. Metals Hard Mater. 29 (2011) 586–590.
[22] W. Wan, J. Xiong, M. Liang, Effects of secondary carbides on the microstructure, mechanical properties and erosive wear of Ti (C, N)-based cermets, Ceram. Int. 43 (2017) 944–952.
[23] W. Wan, J. Xiong, M. Yang, Z. Guo, G. Dong, C. Yi, Effects of Cr3C2 addition on the corrosion behavior of Ti (C, N)-based cermets, Int. J. Refract. Metals Hard Mater. 31 (2012) 179–186.
[24] P. Li, J. Ye, Y. Liu, D. Yang, H. Yu, Study on the formation of core–rim structure in Ti (CN)-based cermets, Int. J. Refract. Metals Hard Mater. 35 (2012) 27–31.
[25] S.M. Rafiaei, A. Bahrami, M. Shokouhimehr, Influence of Ni/Co binders and Mo2C on the microstructure evolution and mechanical properties of (Ti0. 93W0. 07) C–based cermets, Ceram. Int. 44 (2018) 17655–17659.
[26] S. Huang, K. Vanmeensel, H. Mohrbacher, M. Woydt, J. Vleugels, Microstructure and mechanical properties of NbC-matrix hardmetals with secondary carbide addition and different metal binders, Int. J. Refract. Metals Hard Mater. 48 (2015) 418–426.
[27] E. Chicardi, F. Gotor, V. Medri, S. Guicciardi, S. Lascano, J. Córdoba, Hot-pressing of (Ti, Mt)(C, N)–Co–Mo2C (Mt= Ta, Nb) powdered cermets synthesized by a mechanically induced self-sustaining reaction, Chem. Eng. J. 292 (2016) 51–61.
[28] J.M. Córdoba, E. Chicardi, R. Poyato, F.J. Gotor, V. Medri, S. Guicciardi, C. Melandri, Spark plasma sintering of TixTa1− xC0. 5N0. 5-based cermets: effects of processing conditions on chemistry, microstructure and mechanical properties, Chem. Eng. J. 230 (2013) 558–566.
[29] E. Chicardi, Y. Torres, J. Córdoba, M.J. Sayagués, J. Rodríguez, F. Gotor, Effect of sintering time on the microstructure and mechanical properties of (Ti, Ta)(C, N)-based cermets, Int. J. Refract. Metals Hard Mater. 38 (2013) 73–80.
[30] E. Chicardi, Y. Torres, M.J. Sayagués, V. Medri, C. Melandri, J. Córdoba, F. Gotor, Toughening of complete solid solution cermets by graphite addition, Chem. Eng. J. 267 (2015) 297–305.
[31] C. Liu, N. Lin, Y. He, Influence of Mo2C and TaC additions on the microstructure and mechanical properties of Ti (C, N)-based cermets, Ceram. Int. 42 (2016) 3569–3574.
[32] W.T. Kwon, J.S. Park, S. Kang, Effect of group IV elements on the cutting characteristics of Ti (C, N) cermet tools and reliability analysis, J. Mater. Process. Technol. 166 (2005) 9–14.
[33] J. Jung, S. Kang, Effect of nano-size powders on the microstructure of Ti (C, N)-xWC-Ni cermets, J. Am. Ceram. Soc. 90 (2007) 2178–2183.
[34] J. Navarrete-Cuadrado, T. Soria-Biurrun, L. Lozada-Cabezas, F. Ibarreta-López, R. Martínez-Pampliega, J.M. Sánchez-Moreno, Effect of pressure on sintering of TiC-Fe-Cr-Mo cermets under vacuum conditions, Int. J. Refract. Metals Hard Mater. 114 (2023) 106262.
[35] D. Shetty, I. Wright, P. Mincer, A. Clauer, Indentation fracture of WC-Co cermets, J. Mater. Sci. 20 (1985) 1873–1882.
[36] S. Huang, J. Vleugels, B.T. Altintas, J. Huang, B. Lauwers, J. Qian, Microstructure and mechanical properties of WC and Ti (C0. 7N0. 3) modified NbC solid solution cermets, J. Alloys Compd. 850 (2021) 156594.
[37] C. Rong, W. Chen, X. Zhang, N. Liu, The development of nano-modified Ti (C, N) cermets, Recent Pat. Nanotechnol. 1 (2007) 145–162.
[38] S. Cardinal, A. Malchere, V. Garnier, G. Fantozzi, Microstructure and mechanical properties of TiC–TiN based cermets for tools application, Int. J. Refract. Metals Hard Mater. 27 (2009) 521–527.
[39] H. Yu, Y. Sun, L. Hu, H. Zhou, Z. Wan, Microstructural evolution of AZ61-10 at.% Ti composite powders during mechanical milling, Mater. Des. 104 (2016) 265–275.
[40] D. Vedel, M. Storozhenko, P. Mazur, V. Konoval, M. Skoryk, O. Grigoriev, M. Heaton, A. Zavdoveev, Wetting and interfacial behavior of Fe, Co, Ni on (Ti, Zr, Hf, Nb, Ta) C high entropy ceramics, Open Ceramics 15 (2023) 100393.
[41] G. Zhang, Y. Zheng, W. Zhou, Y. Zhao, J. Zhang, Z. Ke, L. Yu, Microstructure and mechanical properties of Ti (C, N)-based cermets fabricated by in situ carbothermal reduction of TiO2 and subsequent liquid phase sintering, Ceram. Int. 44 (2018) 3092–3098.
[42] D. Dong, W. Yang, X. Xiang, B. Huang, H. Xiong, L. Zhang, K. Shi, Microstructural evolution and phase transition mechanism of Ti (C, N)-based cermets during vacuum sintering process, Ceram. Int. 47 (2021) 8020–8029.
[43] H. Zhou, H. Tao, N. Wu, Y. Li, Y. Yin, F. Luo, Sintering behavior of the Ti (C, N)-based cermets with graphite or diamond additives, Int. J. Appl. Ceram. Technol. 19 (2022) 3191–3201.
[44] Q. Zhou, D. Huang, K. Xu, M. Lou, J. Lv, F. Wang, C. Zhan, T. Tang, K. Chang, Effect of La2O3 addition on microstructure and mechanical properties of TiC-based cermets, Ceram. Int. 49 (2023) 18125–18133.
[45] E. Chicardi, J. Córdoba, M.J. Sayagués, F. Gotor, Inverse core–rim microstructure in (Ti, Ta)(C, N)-based cermets developed by a mechanically induced self-sustaining reaction, Int. J. Refract. Metals Hard Mater. 31 (2012) 39–46.
[46] E. Chicardi, J. Córdoba, M.J. Sayagués, F. Gotor, Absence of the core–rim microstructure in TixTa1− xCyN1− y-based cermets developed from a pre-sintered carbonitride master alloy, Int. J. Refract. Metals Hard Mater. 33 (2012) 38–43.
[47] H. Xiong, Z. you Li, X. Gan, L. Chai, Morphology evolution of TiC-based cermets via different sintering schedules, Ceram. Int. 43 (2017) 5805–5812.
[48] W. Lengauer, J. Garcia, V. Ucakar, K. Dreyer, D. Kassel, H. Daub, Functionally graded hardmetals and cermets, Ceram. Trans. 114 (2001) 249–257.
[49] H.G. Adivi, I. Ebrahimzadeh, M. Hadi, M. Tayebi, The effect of alumina nanoparticles addition on high-temperature wear behavior of intermetallic iron aluminide produced by the spark plasma sintering process, Surf. Rev. Lett. 27 (2020) 2050004.
[50] E. Ghandourah, H. Ahmadian, T. Zhou, A. Sadoun, A. Fathy, M. Atif, A.S. Kumar, G. Weijia, Comprehensive investigation of the impact of milling time on microstructural evolution and tribological properties in Mg-Ti-SiC hybrid composites, Mater. Today Commun. 38 (2024) 107835.
[51] L. Chen, Y. Zhao, J. Jing, H. Hou, Microstructural evolution in graphene nanoplatelets reinforced magnesium matrix composites fabricated through thixomolding process, J. Alloys Compd. 940 (2023) 168824.
[52] X. Long, K. Chong, Y. Su, L. Du, G. Zhang, Connecting the macroscopic and mesoscopic properties of sintered silver nanoparticles by crystal plasticity finite element method, Eng. Fract. Mech. 281 (2023) 109137.
[53] Y. Li, X. Chen, X. Zeng, M. Liu, X. Jiang, Y. Leng, Hard yet tough and self-lubricating (CuNiTiNbCr) Cx high-entropy nanocomposite films: effects of carbon content on structure and properties, J. Mater. Sci. Technol. 173 (2024) 20–30.
[54] A. Mostajeran, R. Shoja-Razavi, M. Hadi, M. Erfanmanesh, H. Karimi, Wear behavior of laser cladded WC-FeAl coating on 321 stainless steel substrate, J. Laser Appl. 32 (2020).
[55] H. Karimi, M. Hadi, Effect of sintering techniques on the structure and dry sliding wear behavior of WC-FeAl composite, Ceram. Int. 46 (2020) 18487–18497.
[56] A. Mostajeran, R. Shoja-Razavi, M. Hadi, M. Erfanmanesh, M. Barekat, M. S. Firouzabadi, Evaluation of the mechanical properties of WC-FeAl composite coating fabricated by laser cladding method, Int. J. Refract. Metals Hard Mater. 88 (2020) 105199.
[57] M. Hadi, S.M. Rafiaei, F. Fernandes, The effect of Mo2C additions on the oxidation resistance of (Ti, W) CN cermets as base material for the production of cutting tools, Ceram. Int. 49 (2023) 21538–21545.